ELSEVIER

Contents lists available at ScienceDirect

Estuarine, Coastal and Shelf Science

journal homepage: www.elsevier.com/locate/ecss



Calculating salinity variance fluxes using isohaline coordinates

Linjiang Li^{a, b, c}, Jianrong Zhu^{c, *}, L. Fernando Pareja-Roman ^d

- ^a Department of Atmospheric and Oceanic Sciences & Institute of Atmospheric Sciences, Fudan University, Shanghai, 200438, PR China
- b Innovation Center of Ocean-Atmosphere System Observation and Prediction, Zhuhai Fudan Innovation Institute, Hengqin District, Zhuhai, Guangdong, PR China
- c State Key Laboratory of Estuarine and Coastal Research, East China Normal University, Shanghai, 200062, PR China
- d Department of Civil, Environmental and Ocean Engineering. Stevens Institute of Technology. Hoboken, New Jersey, United States

ARTICLE INFO

Keywords: Vertical salinity variance Isohaline total exchange flow framework Budgets Advection The changiang estuary

1. Introduction

Estuarine dynamics have long been studied from tidally-averaged and tidally-varying perspectives. Steady-state theory (Hansen and Rattray, 1965) indicates that the exchange flow is proportional to depth and along-channel salinity gradients and inversely proportional to the eddy viscosity. The mean velocity and salinity profiles produce a landward, residual salt flux that is consistent with the gravitational circulation (Lerczak et al., 2006). This landward salt flux can be offset by the river discharge, which tends to push the salt seaward. By equating these opposing fluxes, it can be shown that the salt intrusion length depends on basin geometry and mixing (Aristizabal and Chant, 2013; Monismith et al., 2002; Ralston and Geyer, 2019). Wind can also affect the distribution of salinity by Ekman transport (Li et al., 2012; Wang, 1979; Zhu et al., 2020), wind straining (Chen and Sanford, 2009; Scully et al., 2005) and direct wind mixing (Chen and Sanford, 2009; Li et al., 2006). From a tidally-varying point of view, the evolution of stratification and mixing over tidal cycles has been studied through the lens of the potential energy anomaly and turbulent kinetic energy budgets (Simpson et al., 1990). Mixing erodes stratification through shear pro-

ABSTRACT

Vertical salinity variance (SV) budgets are derived using the isohaline Total Exchange Flow (TEF) framework, with the advection of vertical SV quantified by the dispersion of salinity classes across sections. A numerical model of a bifurcated estuary, the Changjiang Estuary, is used to demonstrate the application of this method. The analysis is focused on the North Channel (NC) segment, where strong stratification is produced during neap tides. A notable finding is that the advection of vertical SV is stronger than the advection of horizontal SV during the early neap tides due to the landward excursion of stratified water. However, strong northerly winds can significantly decrease the contribution of advection of vertical SV but increase the advection of horizontal SV into the NC due to landward transport of relatively well-mixed saline water. This process increases the seaward advection of vertical SV in the southern channels. In addition, it is found that the vertical SV dissipation (mixing) balances the straining and reaches maximum at late neap tides in the NC, coinciding with the maximum volume-integrated vertical SV.

duction by tidal currents while the exchange flow acts as a buoyancy flux that stabilizes the water column. This competition between stabilizing and destabilizing components explains the Strain-Induced Periodic Stratification, also introduced by Simpson. The spring-neap cycle involves additional changes in stratification and mixing with implications for the magnitude of the exchange flow at fortnightly timescales. While much has been learned about the spring-neap and ebb-flood variability of straining and exchange, recent studies have broadened the scope by considering the spatiotemporal heterogeneity of the salt field through the concept of salinity variance, 'SV' (Wang et al., 2017). Here, the SV is the squared standard deviation of salinity in an estuary, which is considered a closed control volume. One of the features of the SV is that the total variance can be divided into vertical and horizontal, which facilitates the analysis of straining and lateral dynamics. Intuitively, stratification can be defined as vertical variance and mixing as the destruction of variance. Advection-dispersion (e.g. transport) equations can be derived for SV, as well as budgets in which the SV volume storage is a function of boundary fluxes and internal decay or mixing (Li et al., 2018). Some estuarine processes can be explained in terms of SV transformations. For example, the estuarine circulation strains the

E-mail address: jrzhu@sklec.ecnu.edu.cn (J. Zhu).

Corresponding author.

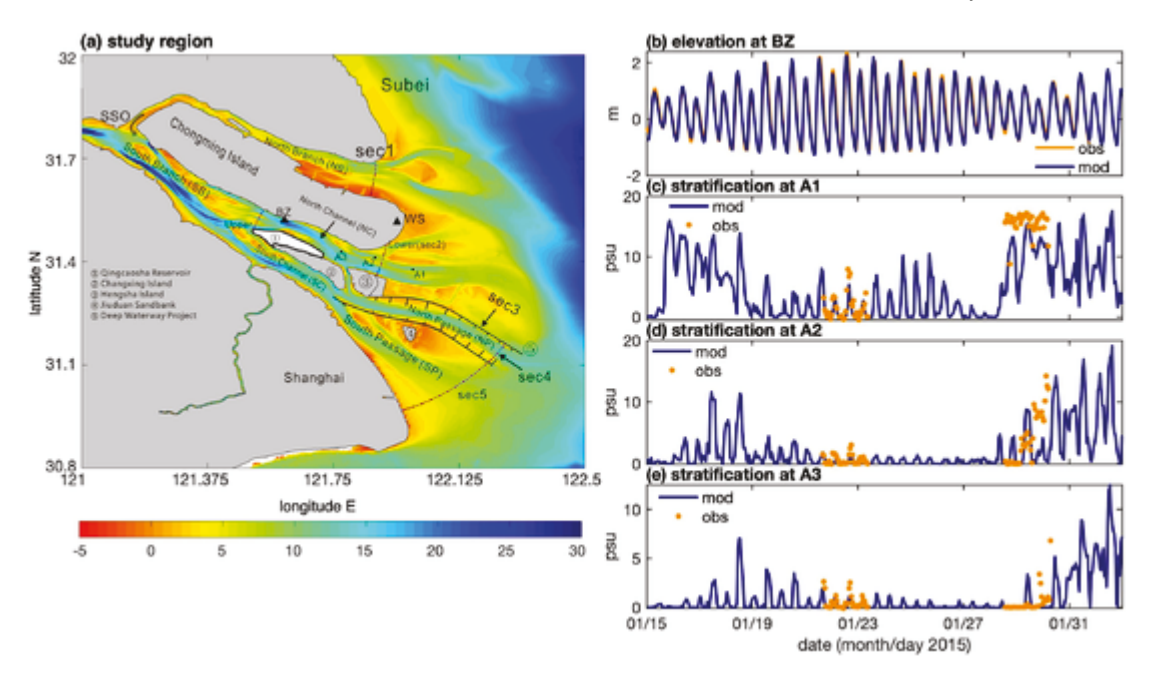


Fig. 1. (a) Bathymetry and features of the Changjiang Estuary. Dashed lines across channels indicate the cross-sections used in this study. Weather and hydrological stations (WS and BZ at Baozhen) are shown, as well as shipboard measurement locations (A1, A2 and A3). (b) Time series of water level at BZ. (c, d and e) modeled and observed stratification at A1, A2, and A3, respectively.

horizontal SV (i.e. the horizontal salinity gradient) into vertical SV (stratification) (Li et al., 2018). The resulting vertical SV can be destroyed by turbulent dispersion. The computation of salt and SV fluxes at control boundaries and cross-sections is key to construct salt budgets in estuaries. MacCready (2011) proposed the 'Total Exchange Flow' (TEF) framework to calculate salt fluxes in isohaline coordinates. The terms used in TEF are reminiscent of the Knudsen (1900) relations for transport (Q) and salinity (S), and employ the subscripts 'in' and 'out' for inflows and outflows, respectively (Q_{in} , Q_{out} , S_{in} , S_{out}). It follows that $Q_{in} + Q_{out}$ is the net volume transport and $Q_{in}S_{in} + Q_{out}S_{out}$ the net salt transport. These terms have been used by many authors (Chen et al., 2012; Giddings and MacCready, 2017; Gräwe et al., 2015; Purkiani et al., 2016; Rayson et al., 2017; Sutherland et al., 2011).

Based on the budgets of SV in the TEF analysis framework, MacCready et al. (2018) derived an approximate quantification for volume-integrated estuarine mixing from the inflow salinity, the outflow salinity, and volume fluxes at the boundaries. The "approximate" expression is used because the errors induced by the nonuniformity of inflow and outflow salinities is ignored in the quantification. In this study, we will quantify the contribution of the nonuniformity of inflow and outflow salinities at the boundaries to the balance of the SV in a wedge estuary, the Changjiang Estuary. We will use the theory of MacCready et al. (2018) and our changed equations in a bifurcate estuary for the first time. In addition, we will consider the effects of winter storm on the balance of SV. To achieve these goals, this article is organized as follows: Section 2 introduces the budgets of SV under isohaline framework, and briefly describe the numerical model setup; section 3 shows the results of the numerical experiments; section 4 presents the discussion; and section 5 lists the conclusions.

2. Methods

2.1. Theoretical framework

First, we revisit the isohaline framework of salinity by MacCready (2011), defining the tidally averaged volume flux of water with salinity greater than s is defined as:

$$Q(s) = \iint_{ds} u \, dA \tag{1}$$

where 'As' denotes the tidally-varying area of the cross section where the salinity is greater than s; dA is the differential of area in the cross-section, and u is the normal velocity. The volume for a given salinity class is obtained by estimating the derivative:

$$\frac{\partial Q}{\partial s} = \lim_{\delta s \to 0} \frac{Q(s + \delta s/2) - Q(s - \delta s/2)}{\delta s} \tag{2}$$

According to the flow direction (e.g. 'in' for landward and 'out' for seaward), the water flux can be divided in inflowing and outflowing components:

$$\begin{aligned} Q_{in} &= \left\langle \int_{A^{+}} \frac{\partial Q}{\partial s} ds \right\rangle \\ Q_{out} &= \left\langle \int_{A^{-}} \frac{\partial Q}{\partial s} ds \right\rangle \end{aligned} \tag{3}$$

where the superscripts (+, -) indicate inflow and outflow, respectively, and the brackets denote a 60-h low-pass filter. The notation "A+", for example, indicates that only inflowing contributions of $\partial Q/\partial S$ are considered in the integral. Following this notation, inflowing and outflowing salt fluxes are given by:

$$Fs_{in} = \left\langle \int_{A^{+}} s \frac{\partial Q}{\partial s} ds \right\rangle$$

$$Fs_{out} = \left\langle \int_{A^{-}} s \frac{\partial Q}{\partial s} ds \right\rangle$$
(4)

It is also convenient to define the flux-weighted salinities as:

$$s_{in} = \frac{Fs_{in}}{Q_{in}}$$

$$s_{out} = \frac{Fs_{out}}{Q_{out}}$$
(5)

Next, we describe the total SV budget in the isohaline TEF framework proposed by MacCready et al. (2018). Considering a three-dimensional domain, for example, an entire estuary, salinity can be decomposed as a volume average (5) and a deviation (5') so that

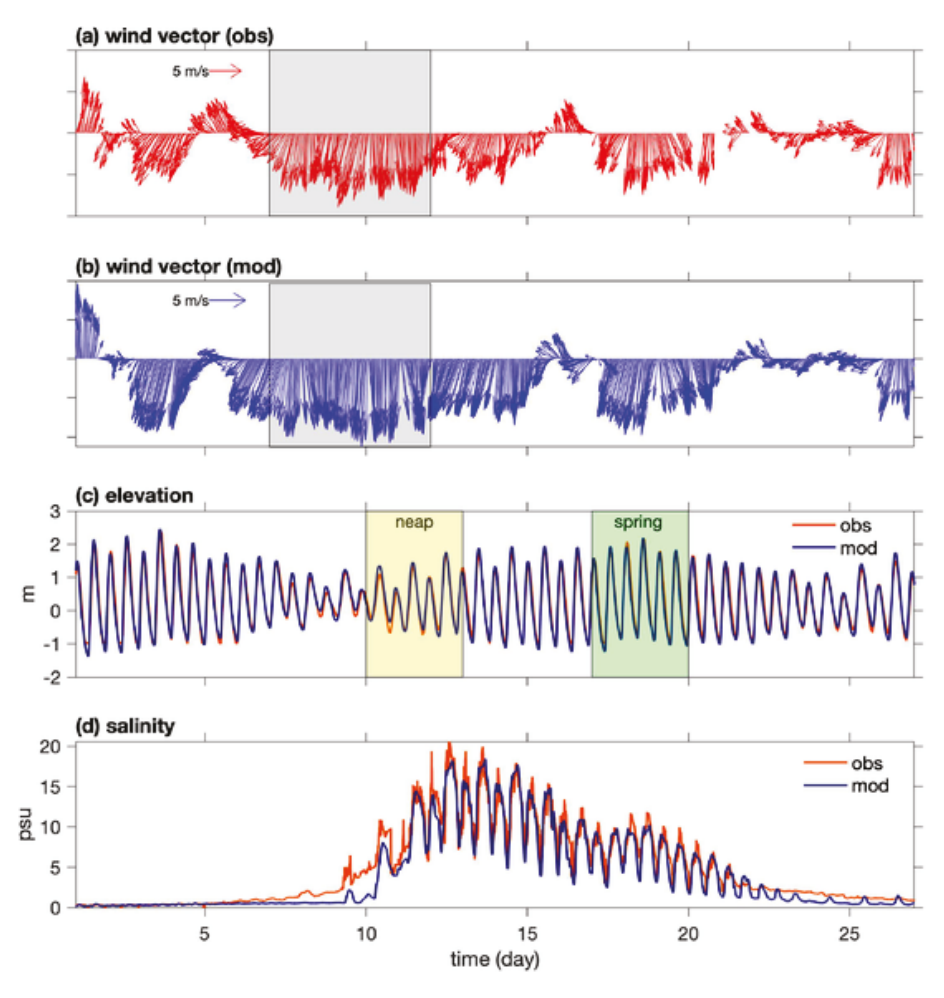


Fig. 2. Time series of (a) observed and (b) modeled wind vectors at WS, and (c) modeled and observed elevation at BZ. Yellow and green boxes show neap and spring tide periods for later analysis. (d) Time series of observed and modeled surface salinity at BZ (bottom salinity was not measured). Model results correspond to the Ex2 scenario. The time axis in this study shows days in February 2014. (For interpretation of the references to color in this figure legend, the reader is referred to the Web version of this article.)

 $S = \bar{S} + S'$. The total SV is defined as $S'^2 = (S - \bar{S})^2$. From the Reynolds-averaged advection–diffusion equation for salinity, the total SV budget in the domain with N boundary sections is:

$$\frac{d}{dt}\left\langle \int \int \int S^{'2} dV \right\rangle = \sum_{i=1}^{N} \left[Q_{in} \left(S^{'2} \right)_{in} + Q_{out} \left(S^{'2} \right)_{out} \right] \Big|_{\sec(i)} - TM \ Q \ (6)$$

where the subscript *i* denotes the number of boundary sections;

$$\left(S'^{2}\right)_{in} = \frac{\left\langle \int_{A^{+}} \left(S - \left\langle \bar{S} \right\rangle \right)^{2} \frac{\partial Q}{\partial s} ds \right\rangle}{Q_{in}}$$

and

$$(S'^{2})_{out} = \frac{\left\langle \int_{A^{-}} (S - \langle \bar{S} \rangle)^{2} \frac{\partial Q}{\partial s} ds \right\rangle}{Q_{out}}$$

are the flux-weighted total variances, and TM is the total mixing, which is the sum of physical (PM) and numerical (NM) mixing. Hereafter, 'mixing' and 'total mixing' are used interchangeably unless otherwise specified. Li et al. (2018) proposed that physical mixing can be computed as $PM = \langle 2 \iiint K(\partial S/\partial z)^2 dV \rangle$, where K is the vertical eddy diffusivity. To better describe the mixing process, Li et al. (2018) also decomposed the total SV into vertical (S'_{V}) and horizontal (S'_{H}) components. New terms then arise in the isohaline TEF framework:

$$\left(S_{h}^{\prime 2}\right)_{in} = \left(S_{in} - \left\langle\bar{S}\right\rangle\right)^{2} \tag{7}$$

$$\left(S_{\nu}^{\prime 2}\right)_{in} = \frac{\left\langle \int_{A^{+}} \left(S - S_{in}\right)^{2} \frac{\partial Q}{\partial s} ds \right\rangle}{Q_{i}} \tag{8}$$

which refer to the flux-weighted horizontal and vertical SV, respectively. After manipulation, it can be proved that (for details see Appendix A):

$$(S'^2)_{in} = (S'^2_h)_{in} + (S'^2_v)_{in}$$
 (9)

Expressions 7–9 also apply to the output salinity variance terms. Then, neglecting lateral gradients, equation (6) can be rewritten as:

$$TM = Straining + \sum_{i=1}^{N} \left[Q_{in} \left(S_{v}^{'2} \right)_{in} + Q_{out} \left(S_{v}^{'2} \right)_{out} \right] \Big|_{\sec(i)} - \frac{d}{dt} \left\langle \iiint S_{v}^{'2} dV \right\rangle$$

Equation (10) summarizes the vertical SV budget in the control volume. The straining term describes the conversion of horizontal SV to vertical SV due to the differential advection of horizontal salinity gradients (Li et al., 2018), and can be written as:

$$Straining = \sum_{i=1}^{N} \left[Q_{in} \left(S_{h}^{'2} \right)_{in} + Q_{out} \left(S_{h}^{'2} \right)_{out} \right] \right] \Big|_{\text{sec}(i)} - \frac{d}{dt} \left\langle \iint S_{h}^{'2} dV \right\rangle (11)$$

The second term on the right-hand-side of (10) is the advective transport of variance across the boundaries. The term $d/dt \left\langle \iiint S'_{\nu}^2 dV \right\rangle$ is the rate of change of net vertical variance. Note also that $\iiint S'^2 dV = \iiint S'_{\nu}^2 dV + \iiint S'_{\nu}^2 dV$ (Li et al., 2018).

In the steady state, conservation of mass implies that:

$$\sum_{i=1}^{N} (Q_{in} + Q_{out}) \bigg|_{\sec(i)} = 0$$
 (12)

$$\sum_{i=1}^{N} (Q_{in}S_{in} + Q_{out}S_{out}) \bigg|_{\sec(i)} = 0$$
(13)

$$\frac{d}{dt} \left\langle \iiint S'^2 dV \right\rangle = \frac{d}{dt} \left\langle \iiint S'_v^2 dV \right\rangle = \frac{d}{dt} \left\langle \iiint S'_h^2 dV \right\rangle = 0 \tag{14}$$

Finally, based on equations (11)–(14), the steady-state mixing term can be written as:

$$TM = \sum_{i=1}^{N} \left(Q_{in}S_{in}^2 + Q_{out}S_{out}^2\right)\Big|_{\sec(i)} + \sum_{i=1}^{N} \left[Q_{in}\left(S_v^{\prime 2}\right)_{in} + Q_{out}\left(S_v^{\prime 2}\right)_{out}\right)\right]$$

2.2. Study region and numerical model

The Changjiang (Yangtze River) Estuary is a large, multi-branch estuary (Fig. 1). Chongming Island divides the estuary into branches, (North and South). The South Branch is further divided by Changxing Island into two channels, the North Channel (NC) and South Channel (SC). The SC is divided by the Jiuduan Sandbank into two passages, the North and South Passages. The annual mean discharge of the Chanjiang Estuary is $30,000~\text{m}^3/\text{s}$. Since the NC is the main freshwater pathway to the coastal ocean (Li et al., 2010), a relatively strong horizontal salinity gradient and stratification develop at its mouth (Li et al., 2018).

Significant saltwater intrusion in the NC is usually observed in the winter when the river discharge drops to about 11,000 m³/s. The landward excursion of salinity is enhanced during neap tides (Li et al.,

2020) and under strong northerly winds (Zhu et al., 2020). Shipboard measurements reveal that strong stratification during neap is usually destroyed during springs tides (Fig. 1, time series). In this study, we focus on the variability of salinity and SV in the NC segment of the Changjiang Estuary.

We use the ECOM-si hydrodynamic model (Blumberg, 1994; Wu and Zhu, 2010), which employs the Mellor-Yamada 2.5 turbulence closure scheme (Mellor and Yamada, 1982). The ECOM-si model of the Changjiang we use here is well-established and validated; see e.g., Wu and Zhu (2010) and Lyu and Zhu (2018). River forcing is based on observations at the Datong hydrological station. The model is forced by sixteen harmonic tidal constituents at the open boundaries. Initial conditions for salinity were obtained from the Ocean Atlas of the Huanghai Sea and East China Sea (Atlas, 1992). More details on the model boundary and initial conditions are provided by Lyu and Zhu (2019). To validate the spring-neap variability of stratification, we compared model results with shipboard measurements during January 2015 (Fig. 1, c-e). Although there are some discrepancies between model and observations, the model successfully captures the transition from weakly stratified spring to strongly stratified neap.

The winter monsoonal circulation induces northerly winds (\sim 6 m/s) in the Changjiang Estuary. Stronger winter winds (>10 m/s) during storms can abnormally increase salt intrusion and salinity (Zhu et al., 2020) and change the salinity structure in the NC (Li et al., 2020). In February 2014, a strong northerly wind event was recorded at the weather station (WS) with maximum wind speeds over 14 m/s, which significantly increased salt intrusion at station BZ (Fig. 2a, d). Two numerical experiments were designed to study the salinity response under climatic and strong, sustained northerly winds. In experiment 1 (Ex1), we force the model with climatic northerly winds of about 6 m/s. In Ex2, we consider a strong northerly wind event observed in February 2014. Wind forcing was obtained from atmospheric model output (Weather Research and Forecasting, WRF; further configuration details are available Li et al. (2014)). Simulated wind vectors at WS are shown in Fig. 2b and show good agreement with observations. Other boundary conditions, including river discharge (11,000 m³/s, close to the

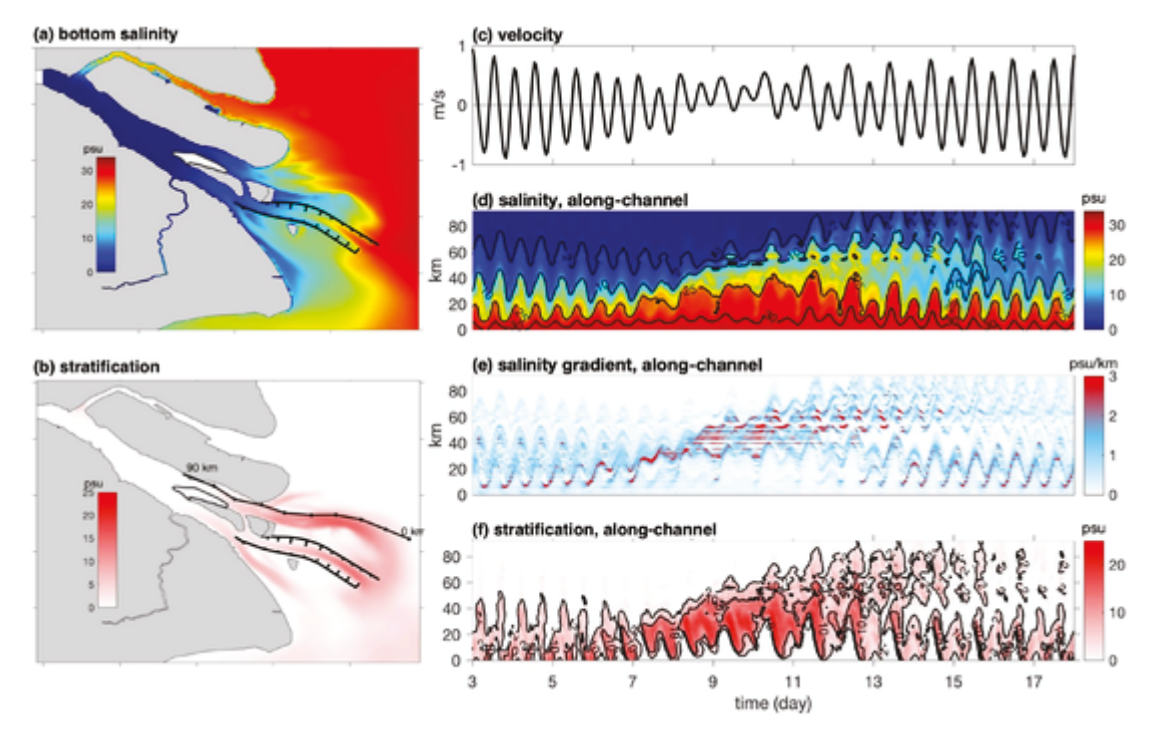


Fig. 3. Model results of (a) mean bottom salinity and (b) stratification during late neap (days 10–13). The black dotted line in (b) is the along-channel coordinate 'SecNC' that is used in (d–f). (c) bottom velocity at km 50 along the channel (flood positive), time series of along-channel (d) bottom salinity, (e) bottom salinity gradient, and (f) stratification. All the results are from scenario Ex1.

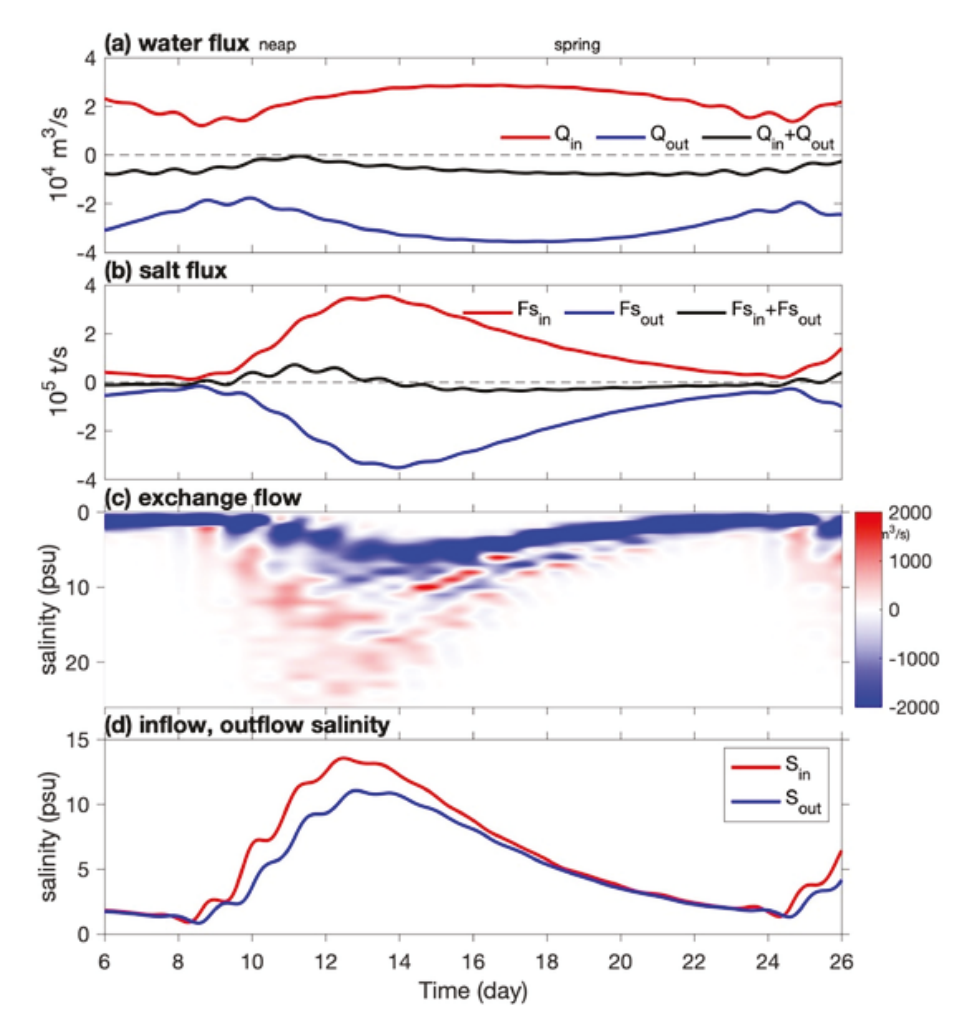


Fig. 4. Time series of (a) water flux (equation (3)), (b) salt flux (equation (4)), (c) exchange flow $\langle \partial Q/\partial S \rangle$, and (d) representative inflow and outflow salinity (equation (5)) at the mouth of the NC.

monthly mean river discharge in February 2014), are the same in both experiments.

3. Results

Here we describe the salinity response in the estuary under climatic and strong northerly winds through the lens of salinity variance and TEE

3.1. Salinity response under climatic winds

Fig. 3a and b shows the mean bottom salinity and stratification from days 10–13 (neap tide in Ex1). The river discharge creates a strong, stratified salinity front (\sim 20 psµ) at the mouth of the NC. The right panels in Fig. 3 show that the stratified front moves landward along the NC from days 7–13 when tidal currents are weak (the along-channel NC coordinate, SecNC, is the black dotted line in Fig. 3b). The landward advection of the front is halted as the tidal current speed increases after day 13.

Volume and salt transports at the mouth of the NC exhibit spring-neap variability (Fig. 4). The net seaward water flux ($Q_{in} + Q_{out}$) is minimum (\sim 1100 m³/s) on day 11 during neap and maximum at day 19 during spring (\sim 8600 m³/s). This occurs because the water diversion ratio of the NC is smaller than that of the SC during neap (Li et al., 2010). The salt flux ($Q_{in}S_{in} + Q_{out}S_{out}$) is landward from days 10–14 (Fig. 4b) because the seaward water flux in the NC is smaller in neap than in spring (Fig. 4a and b). In addition, the landward salt flux ex-

change is stronger in neap (Li et al., 2020), similar to other partially stratified estuaries (e.g., Hudson Estuary (Bowen and Geyer, 2003; Lerczak et al., 2006); Pearl River Estuary (Gong and Shen, 2011)). Fig. 4c shows the inflow and outflow at different salinities. High-salinity water (max \sim 26 psµ) enters the NC while relatively low-salinity water leaves the NC during neap, which is a classic characteristic of estuarine circulation when tidal stirring is weak (Geyer and MacCready, 2014). The flux-weighted peak salinities of the inflow and outflow are about 13 and 10 psµ, respectively, both appearing at late neap. Starting on day 14, given the larger seaward water flux and stronger tidal stirring, the net salt flux is seaward and the minimum flux-weighted salinities of inflow and outflow both decrease below 3 psµ.

Neap-averaged volume transports across the lower section (days 10–13) are binned in different salinity classes as shown in Fig. 5a. Both inward and outward volumes have strong salinity deviations with a range from 1 to 26 psµ. This feature corresponds with the strong stratification in the lower section, as Fig. 5c illustrates. The difference in flux-weighted salinity between inward and outward volumes is about 3 psµ during neap. In contrast, inflow and outflow salinity classes range from 2 to 9 psµ during spring (days 17–20). In spring, the difference in flux-weighted salinity between inflow and outflow decreases to 0.4, indicating a relatively well-mixed status (Fig. 5d). Overall, the salinity variance across the lower section undergoes significant springneap variability, from $15 \text{ ps}\mu^2$ in neap to $1 \text{ ps}\mu^2$ in spring. Next, we multiply the tidal variance and volume across the boundaries to obtain the SV flux advection to the NC segment.

During early neap (days 8–10), the advection of vertical SV into the NC is stronger than of horizontal SV, which means that the stratified saline water intrusion brings more stratification than the along-channel salinity gradient into the NC (Fig. 6). The maximum vertical SV is $2.6 \times 10^5 \ \text{ps} \mu^2 \ \text{m}^3/\text{s}$ on day 11. After day 11, the horizontal SV flux is larger than the vertical with an increase in the landward salt flux. Both the horizontal and vertical SV decrease during spring tide because of the weak saltwater intrusion into the NC (Fig. 3d). The total SV flux at the upper boundary is dominated by the horizontal SV (Fig. 6c), as the salinity and stratification at that location is close to 0 (Fig. 3a and b). The advection of horizontal SV into the NC from the upper section is maximum at the late neap when there is maximum saltwater intrusion in the NC.

Flux-weighted inflow and outflow variances are shown in Fig. 6b and d. During neap, both horizontal and vertical variances increase when the stratified saline water moves landward. Note that the vertical variance of the inflow is slightly higher than the horizontal variance, which is reversed for the outflow (Fig. 6b). The maximum $\left(S_{\nu}^{\prime\,2}\right)_{in}$ is 25 ps μ^2 whereas the maximum $\left(S_{\nu}^{\prime\,2}\right)_{out}$ is 15 ps μ^2 , which indicates that the water with higher vertical variance is mixed inside the segment and exits to the coastal ocean with lower vertical variance. Both vertical and horizontal flux-weighted variances are higher at the lower boundary than at the upper. The vertical SV at the upper boundary is negligible most of the time, indicating the presence of a stationary river boundary where salinity and stratification are zero.

The evolution of vertical variance budget terms (equation (10)) are shown in Fig. 7a. We find that the advection of vertical SV across the boundary is much stronger than the straining at the beginning of the neap tide (days 9–11). Stated differently, the early neap stratification in the segment arises from advection across the boundary rather than from local re-stratification. In late neap, the straining is stronger than the vertical SV advection, which means that stratification in the segment develops mainly from the straining of the horizontal SV rather than from the advection across the boundary. The rate of change in the net vertical SV (equation (10)) is positive during the neap, which means

that the vertical SV from straining and advection exceeds the dissipation from tidal mixing. The opposite is observed during spring tides under stronger tidal stirring. The advection (during early neap), straining (during late neap) and mixing are the dominant terms in the vertical SV balance, while the rate of change in the net vertical SV is relatively small. The maximum mixing is $8.4 \times 10^5 \ \text{ps} \mu^2 \ \text{m}^3/\text{s}$ is observed in late neap tide when the volume-integrated vertical SV is maximum (Fig. 7b).

In steady-state, the rate of change in net SV is zero (equation (14)); thus, mixing can be quantified by the variance advection across the boundaries as equation (15) shows. The values of the mean TEF terms (from days 6–21) at the boundaries of the NC are shown in Table 1. Values of $Q_{in}S_{in}^2+Q_{out}S_{out}^2$ at the upper and lower sections are 570 psµ² m³/s and 5.6 × 10⁴ psµ² m³/s, respectively. The variance flux $Q_{in}(S_{v}^{\prime 2})_{in}+Q_{out}(S_{v}^{\prime 2})_{out}$, also at upper and lower sections, are 750 psµ² m³/s and 4.4 × 10⁴ psµ² m³/s. Steady-state mixing in the NC is then 1.2×10^4 psµ² m³/s, which mainly is determined by the TEF terms at the lower section.

3.2. Salinity response under strong northerly winds

Previous studies showed that strong northerly winds (> 10 m/s) favor the landward advection of saltwater in to the NC (Zhu et al., 2020). An example of such a response can be seen during the strong wind event of February 2014 when the salinity at BZ increased dramatically (Fig. 2d). Fig. 8a and b shows the modeled bottom salinity and stratification averaged from days 10–13 during neap tide (scenario Ex2). Model results show that the salinity in the NC increases significantly under the strong northerly wind, and that the stratification moves landward into the NC. However, the stratification is weaker (\sim 10 ps μ) relative to the climatic wind scenario (\sim 20 ps μ , Fig. 3b). The net seaward water flux ($Q_{in} + Q_{out}$) is landward from days 9–14 under strong winds condition, and the maximum landward flux at the lower section about

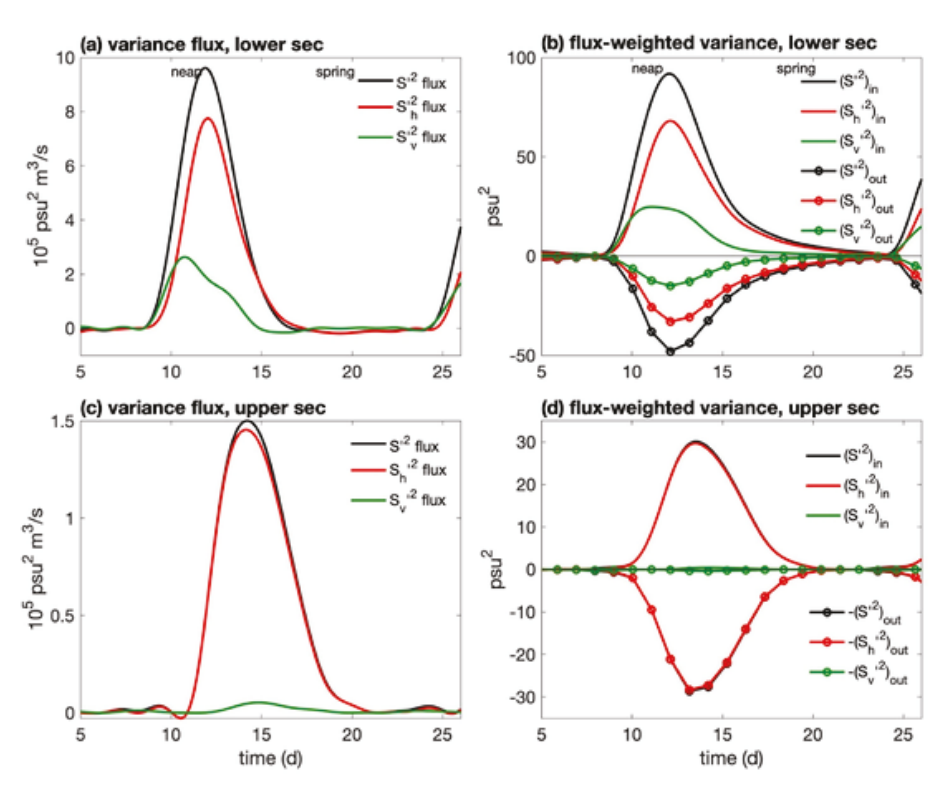


Fig. 6. Variance fluxes and flux-weighted variances at (top, a,b) lower section and (bottom, c,d) upper section.

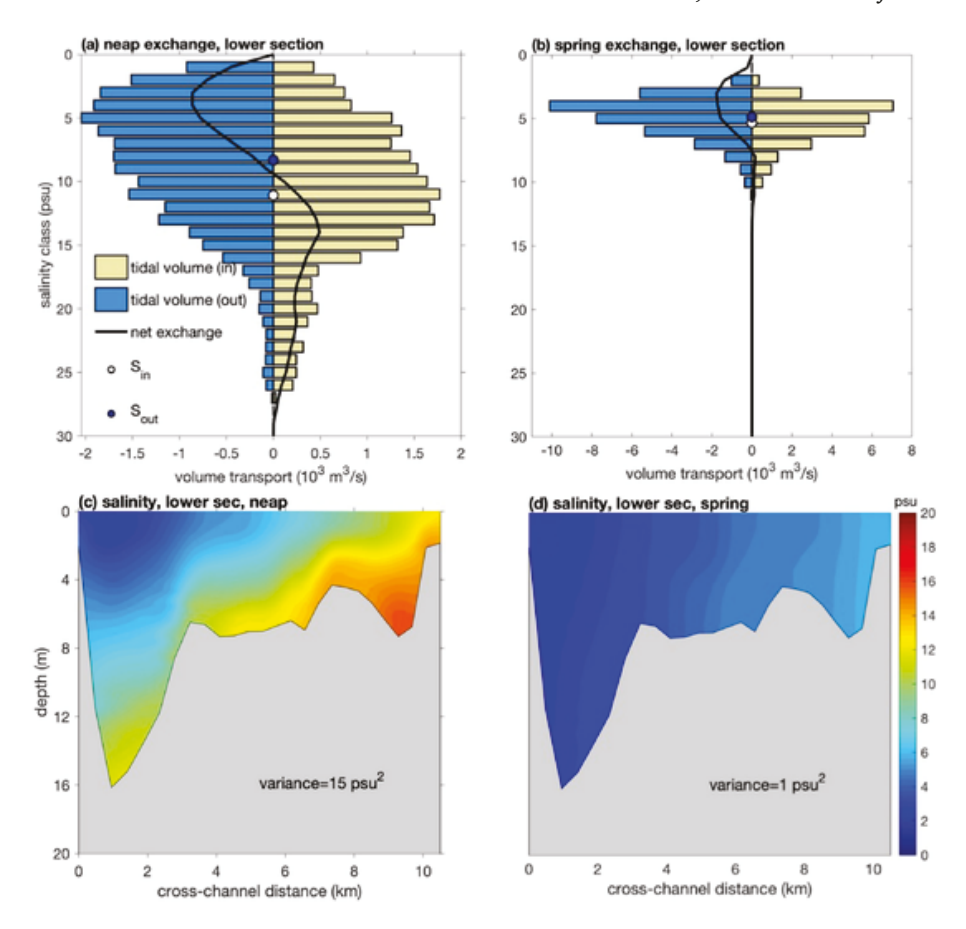


Fig. 5. Exchange flow profiles at the lower section during (a) neap and (b) spring tides. Volume transports are binned in different salinity classes (bin size $1 ps\mu$). The net exchange profile (black line) is obtained by adding the blue and yellow bars for each class. Flux-weighted salinities are denoted by white (inflow) and blue (outflow) markers. Cross-channel salinity at the lower section averaged during (c) neap and (d) spring. The cross-channel coordinate goes from south to north. (For interpretation of the references to color in this figure legend, the reader is referred to the Web version of this article.)

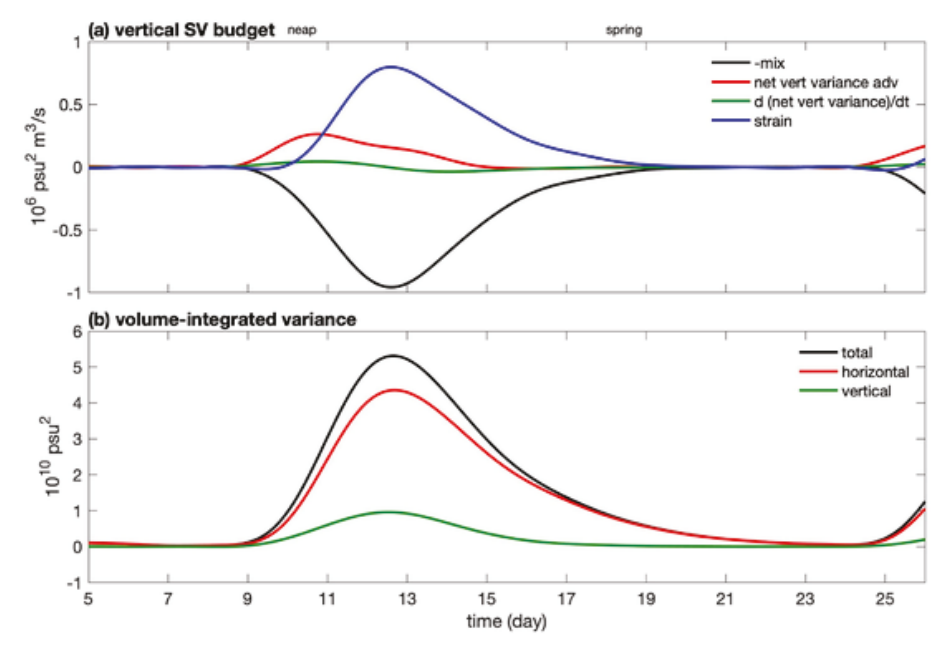


Fig. 7. (a) Terms in the vertical SV budget (equation (10)), where net vert variance adv is $\sum_{i=1}^{N} \left[Q_{in} (S_{v}^{\prime 2})_{in} + Q_{out} (S_{v}^{\prime 2})_{out} \right]_{sec(i)}^{l}$, d(net vert variance)/dt is $\frac{d}{dt} \left\langle \iiint S_{v}^{\prime 2} dV \right\rangle$. Strain is calculated by equation (11). Note mix is total mixing (NM), which is calculated by the other three terms in equation (10). (b) Time series of volume-integrated variance.

Table 1
Mean values of the TEF terms from day 6–21 at NC boundaries.

	$Q_{in} (m^3/s)$	Q_{out} (m^3/s)		S _{out} (psu)	$\left(S_{v}^{\prime2}\right)_{in}(\mathrm{psu}^{2})$	$\left(S_{v}^{\prime2}\right)_{out}(\mathrm{psu^2})$
Lower section	2.4×10^4	-3.0×10^{4}	4.9	4.1	6.0	3.4
Upper section	2.7×10^4	-2.1×10^4	0.4	0.4	0.07	0.07

 $1.0\times10^4~m^3/s$ (Fig. 8c). During this period of landward transport, a salt front moves landward into the NC. Stratified saline water reaches km 80 along the NC (Fig. 8f), which is farther upstream than the intrusion in the climatic wind condition (Fig. 3f).

The neap-averaged volume transport across the lower section is binned in salinity classes as shown in Fig. 9a. The salinity for both the inflowing and outflowing volumes ranges from 10 to 30 ps μ . Under strong winds, the difference in flux-weighted salinity is 1.3 ps μ , about half the difference observed in the climatic wind scenario. This feature

corresponds with a relatively weak stratification in the lower section under strong winds (Fig. 9b). Overall, the salinity deviation across the lower section is smaller in the strong wind experiment due to the wind-induced stirring. The averaged variances from days 10–13 are approximately 10 ps μ^2 and 15 ps μ^2 in Ex2 and Ex1, respectively.

Under climatic winds, the advection of vertical SV at the lower section is stronger than of horizontal SV for about two days during early neap. Under the strong winds, however, this period is less than a day. In addition, the inflowing vertical SV is always smaller than the horizontal (Fig. 10b). All of these features demonstrate that weakly stratified saline water is advected into the NC at the lower section under the strong northerly winds in February 2014. This process increases the advection of horizontal SV with a maximum value of $1.7\times10^4~\rm ps\mu^2~m^3/s$, which is about twice the number under the climatic winds.

At the upper section, there is an outward advection of horizontal SV from days 9–11. This is because the landward residual currents at this

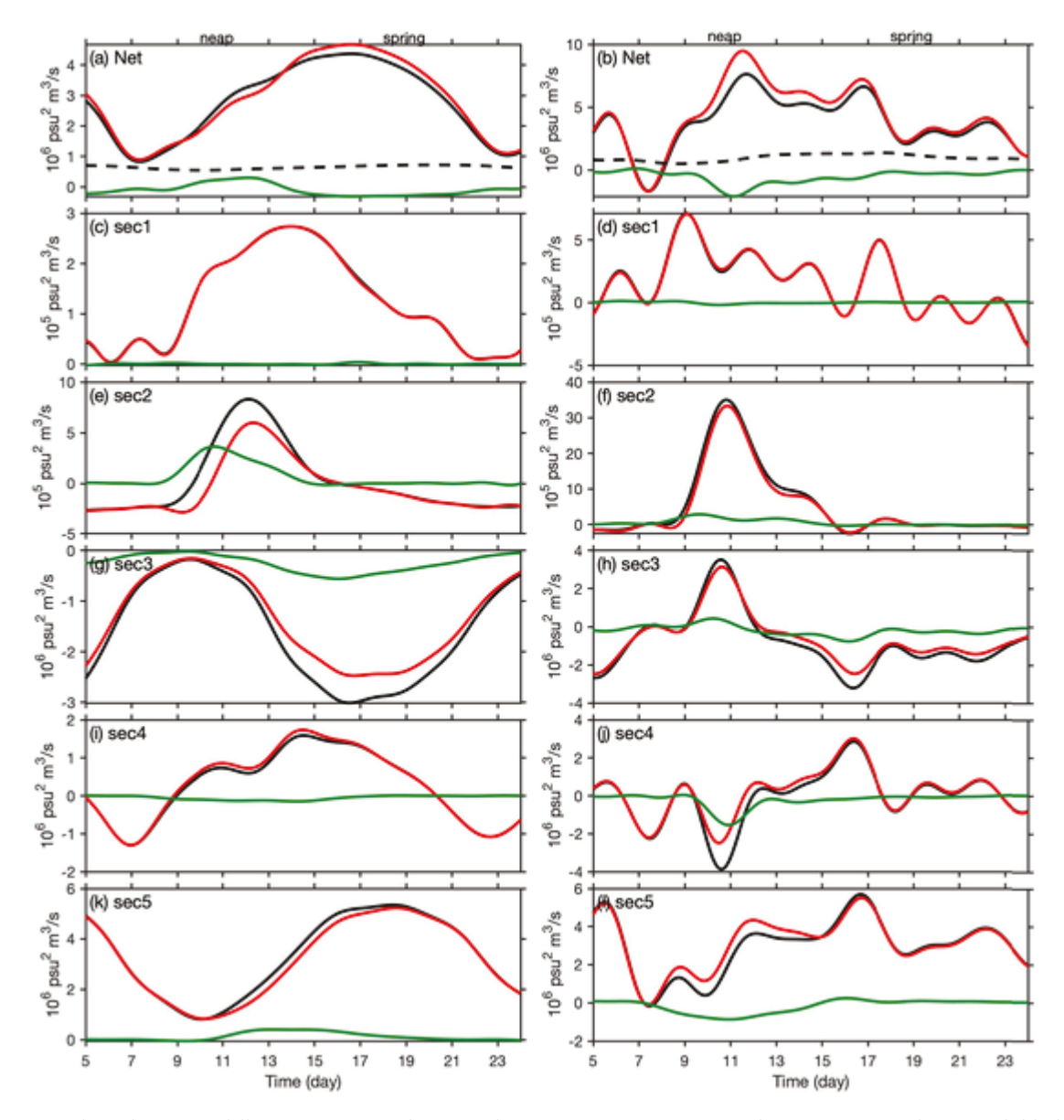


Fig. 12. Time series of SV advection at different sections. For the section locations, see Fig. 1. Variance advection terms are shown: total (black), horizontal (red) and vertical (green). In (a) and (b), the black dashed line represents the variance input via river discharge, and the net value represents the total of all sections, including river input. The left panel shows the results from Ex1 (climatic winds), and the right panel shows the results from Ex2 (strong winds). (For interpretation of the references to color in this figure legend, the reader is referred to the Web version of this article.)

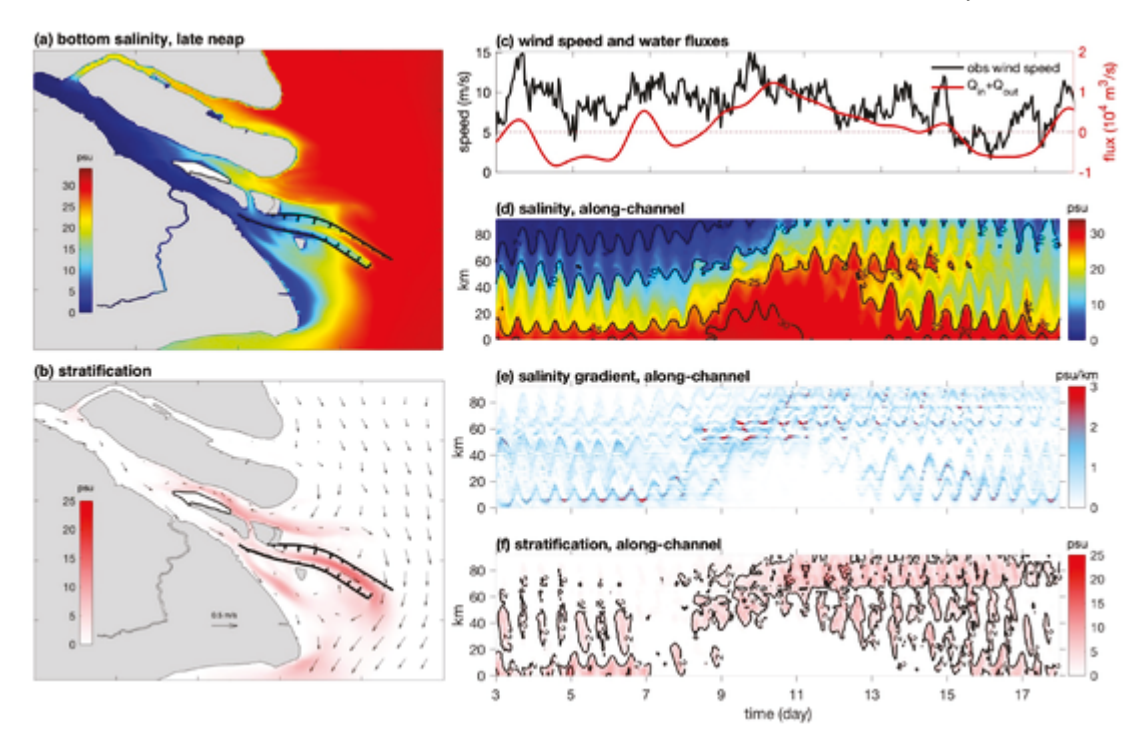


Fig. 8. (a) Modeled bottom salinity distribution at late neap tide in Ex2. (b) Depth-averaged currents (arrows) and stratification (color coded) during neap tides. (c) Time series of observed wind speed at WS (black) and water flux at the lower section. Time series of along-channel (d) bottom salinity, (e) bottom salinity gradient, and (f) stratification. (For interpretation of the references to color in this figure legend, the reader is referred to the Web version of this article.)

section bring the saline water that leaves the NC segment (Fig. 8b). Because the stratified saline water reaches the Upper section under the strong north wind, both $\left(S_{\nu}^{\prime 2}\right)_{in}$ and $\left(S_{\nu}^{\prime 2}\right)_{out}$ at the Upper section are bigger than zero, whereas they are almost zero under the climatic wind.

Time series of the terms in the vertical variance budget (Equation (10)) under the strong north wind in February 2014 are shown in Fig. 11a. It is found that straining and mixing are the dominant terms in the vertical SV balance, advection and the rate of change in the net vertical SV are not dominant terms in the vertical SV balance. In other words, the relatively wellmixed saline water is advected into the NC under the strong north wind, which increases the horizontal salinity gradient and horizontal SV in the NC. The vertical SV in the NC is mainly from the straining of horizontal SV and the contribution of the advection of vertical SV across the boundaries can be neglected compared with that in the climatic wind. The maximum mixing in the Ex2 is 1.6×10^6 psµ 2 m 3 s $^{-1}$, which is about 1.7 times that under climatic wind condition (9.6 \times 10⁵ ps μ 2m³s⁻¹). This is because the maximum volume-integrated vertical SV in Ex2 (2 \times 10¹⁰ ps μ ², see Fig. 11b) is about 2 times that under climatic wind condition (9.6 \times 10⁹ psµ²).

3.3. SV budgets for all the channels of the Changjiang Estuary

After analyzing SV budgets in the NC, we now consider the whole estuary. We choose six boundaries to close the entire estuary: sec1 is located at the mouth of the North Branch; sec2 is located at the mouth of the NC (the Lower section); sec3 is located along the north dyke of the Deep Water Project; sec4 is located at the mouth of the North Passage; sec5 is located at the mouth of the South Passage (the locations are shown in Fig. 1a using purple dashed lines); and a river boundary is located upstream of the North Branch and South Branch junction, where the salinity is 0.

The advection of SV is shown in Fig. 12. We examine the sum (net) of all sections under the climatic wind condition first (Fig. 2a). It is

found that the advection of horizontal SV into the Changjiang Estuary increases from 0.8×10^6 (psu² m³/s) at the early neap (Day 7) to \sim 4.7 \times 10⁶ (s² m³/s) at the early spring tide (Day 17). The advection of vertical SV is inward during neap tide and outward during spring tide and the magnitude is much smaller than the Horizontal SV. The contribution of advection across sec1 to the net SV advection is relatively small, as the North Branch is a shallow and narrow channel with less than 5% river discharge entering into (Lyu and Zhu, 2018; Xue et al., 2009; Zhang et al., 2019). The advection of vertical SV from sec2 is an important source of the net vertical SV advection. Outward advection of vertical and horizontal SV due to tide-induced northward transport (Li et al., 2020; Wu et al., 2010) at sec3 is important for the export of vertical and horizontal SV for the whole estuary. The advection of horizontal SV into the SC at sec5 during spring tide is important for the import of horizontal SV for the whole estuary as the landward Stokes transport is strong during spring tide (Wu et al., 2010). The advection of vertical SV at sec5 is also an import source for the import of net vertical SV into the Changjiang Estuary from Day 11-17 during the transition time from neap to spring tide.

The SV advection shows a different pattern under the strong north wind conditions in Ex2. As Fig. 12a shows, the maximum import of net horizontal SV (9.5 \times 10⁶ (psu² m³/s)) appears at day 12 because of landward Ekman transport induced by the strong north wind in February 2014. Interestingly, there is a relatively strong export of vertical SV $(-2.1 \times 10^6 \text{ (psu}^2 \text{ m}^3/\text{s)})$ at Day 11. A large increase in the SV input is observed at the mouth of the NC (sec2) and becomes an important source of the net horizontal SV advection, but the vertical SV inputs disappear, which is strong in Ex1. Under the strong north wind conditions, a notable SV input is observed across sec3 during the neap tide, which disappears during the spring tide. During neap tides, the winddriven southward transport surpasses the northward tidal transport, causing a net SV input. The opposite conditions occur during spring tides. Similar to the NC, the vertical SV advection is small due to wind stirring. However, there is an export of vertical SV at sec4 and sec5 from Day 10-13, which contributes most of the export of the net verti-

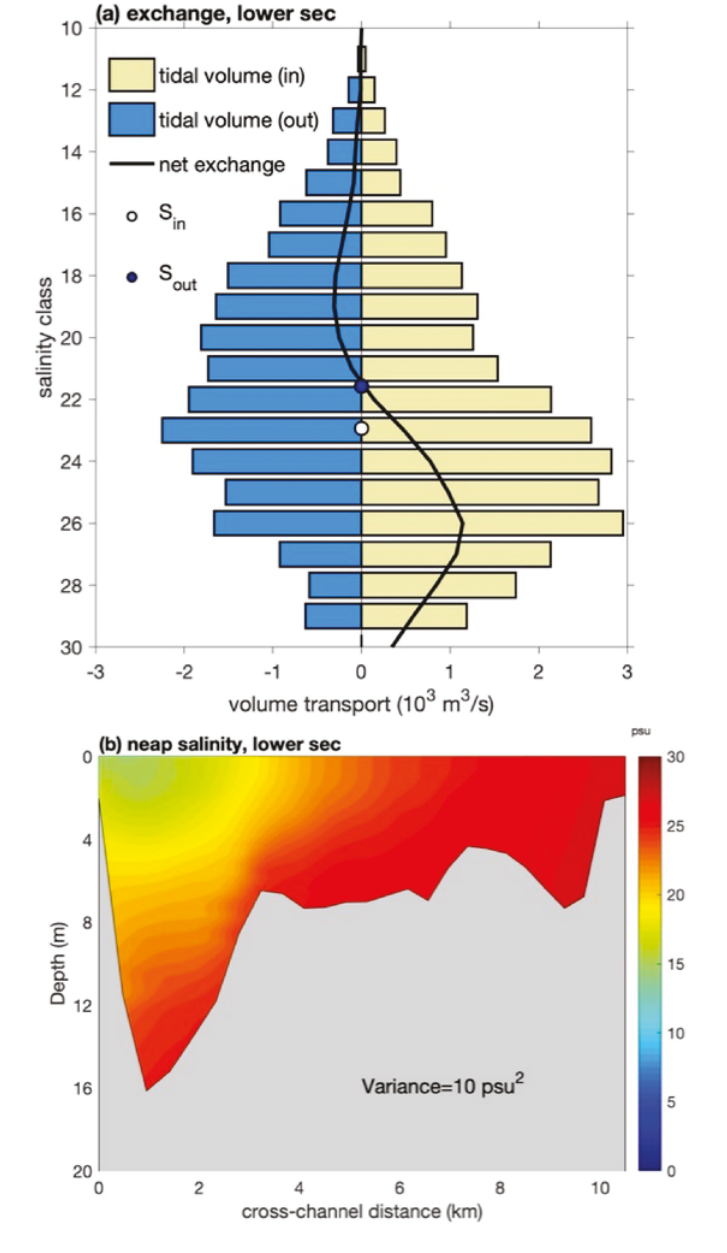


Fig. 9. (a) Exchange flow and flux-weighted salinities in the lower section. (b) Salinity distribution at the lower section during neap tide.

cal SV of the Changjiang Estuary. The reason for this phenomenon is the wind-induced horizontal circulation (Li et al., 2020; Wu et al., 2010; Zhu et al., 2020), which prevents the river discharge entering into the NC and increases the seaward currents in the SC, North Passage and South Passage. With a stronger river discharge entering into the North Passage and South Passage, there is a relatively strong stratification at the lower reach of North Passage and South Passage comparing with the results in Ex1 (see Figs. 3b and 8b). The stratification has not been completely destroyed by wind and tide stirring, which carries the vertical variance out of the North Passage and South Passage and into the plume, and this phenomenon disappears during the spring tide.

The time series of the terms in the vertical variance budget (Equation (10)) for the whole estuary are shown in Fig. 13a (climatic wind condition) and Fig. 13b (strong north wind condition). It is found that straining and mixing are the dominant terms in the vertical SV balance, advection and the rate of change in the net vertical SV are not dominant terms in the vertical SV balance. In the Ex1, the maximum mixing of the whole estuary appears at Day 18 during spring tide with the

value of $3.6 \times 10^6 \ \text{ps}\mu^2 \text{m}^3 \text{s}^{-1}$, which is ~ 4 times that in the NC. The spring-neap variation in the straining and mixing in the whole estuary is not obvious compared with that in the NC (Fig. 7a). However, strong northerly wind events can increase the variation of mixing in the whole estuary, which is $1.7 \times 10^6 \ \text{ps}\mu^2 \text{m}^3 \text{s}^{-1}$ on day 7 when the strong wind begins and increases to $6.7 \times 10^6 \ \text{ps}\mu^2 \text{m}^3 \text{s}^{-1}$ on day 12.

4. Discussions

4.1. Comparison to other studies

This study is based on the theory of MacCready et al. (2018), which proposed a simple equation to calculate the time-averaged and volume-integrated estuarine mixing as $TM = Q_r S_{in} S_{out}$. However, there are some limitations and assumption regarding this equation. First, it only applies for a control volume with two boundaries, one of which is a river boundary where ($S_{in} = S_{out} = 0$). In this study, we do not need the condition that one of the boundaries should be a river. For example, the salinity at the upper boundary is not zero in Ex2 (Fig. 8a). We extend the case from two boundaries in previous studies to N boundaries (Equations (6), (10) and (15)), which is suitable for bifurcated estuaries. MacCready et al. (2018) also indicated that errors in that simple equation for TM result from the slight deviation from the assumption of uniform inflow and outflow salinities. To reduce these errors, the ocean boundaries should be chosen as the vertically well mixed sections. In real situations, however, this condition is hard to satisfy. Here, we quantify contribution of the deviation of the inflow and outflow salinities to the SV balance by $\left(S_{v}^{\prime2}\right)_{in}$ and $\left(S_{v}^{\prime2}\right)_{out}$, respectively.

In previous studies, it was found that maximum mixing in a partially mixed estuary occurs at the late neap tide (e.g., Hudson River Estuary (Wang and Geyer, 2018); ideal estuary (MacCready et al., 2018)). In this study, we also find that the maximum total mixing in the NC occurs at late neap tide and that the total mixing decreases to zero at the late spring tide. As shown in Fig. 7b, the volume-integrated vertical SV in the NC is almost zero due to the weak saltwater intrusion during spring tide (between days 19 and 25), thus the total mixing is, intuitively, zero (Fig. 7a, black line). As for the physical mixing, more mixing is expected during spring tides when there are swifter tidal currents as well as higher vertical eddy diffusivity. Recall that the physical mixing is calculated as: $PM = \langle 2 \iiint K(\partial S/\partial z)^2 dV \rangle$. However, the physical mixing is not only dependent on K but on $\partial S/\partial z$. We quantify the volume-averaged eddy diffusivity of the NC segment with the turbulence closure scheme and $\partial S/\partial z$ in Ex1. As shown in Fig. 14a, the volume-averaged eddy diffusivity in the NC is $\sim 4.9 \times 10^{-3}$ m²/s during late neap tide (days 12-14), which is about 0.43 times the mean diffusivity from day 21-23 during late spring tide. However, the volumeaveraged $\partial S/\partial z$ from day 12–14 is over an order of magnitude larger than the volume-averaged $\partial S/\partial z$ from day 21–23 (due to a weak saltwater intrusion). As a result, physical mixing is maximum at late neap tide and minimum at late spring tide (Fig. 14c). Overall, the phase of total and physical mixing in the NC is similar to previous studies.

In previous studies, SV budgets were used to quantify numerical mixing (Burchard and Rennau, 2008; Li et al., 2018; MacCready et al., 2018; Wang et al., 2021). Numerical mixing is the result of total mixing minus physical mixing. In scenario Ex1, numerical mixing in all channels is shown in Fig. 14d. We found that the magnitude of numerical mixing is 30% of the total, similar to findings by Li et al. (2018). However, numerical mixing of our results is higher than that in MacCready et al. (2018). The reason could be that the river discharge in our study (11,000 m³/s) is much higher than that (1500 m³/s) in MacCready et al. (2018). The higher river flow will cause a stronger salt gradient. Also, according to Rennau (2011), the numerically induced mixing may be of the same order of the physical mixing when modeling the advection of high density gradients. Wang et al. (2021) also found a higher numerical mixing of salinity inside the Changjiang River plume region.

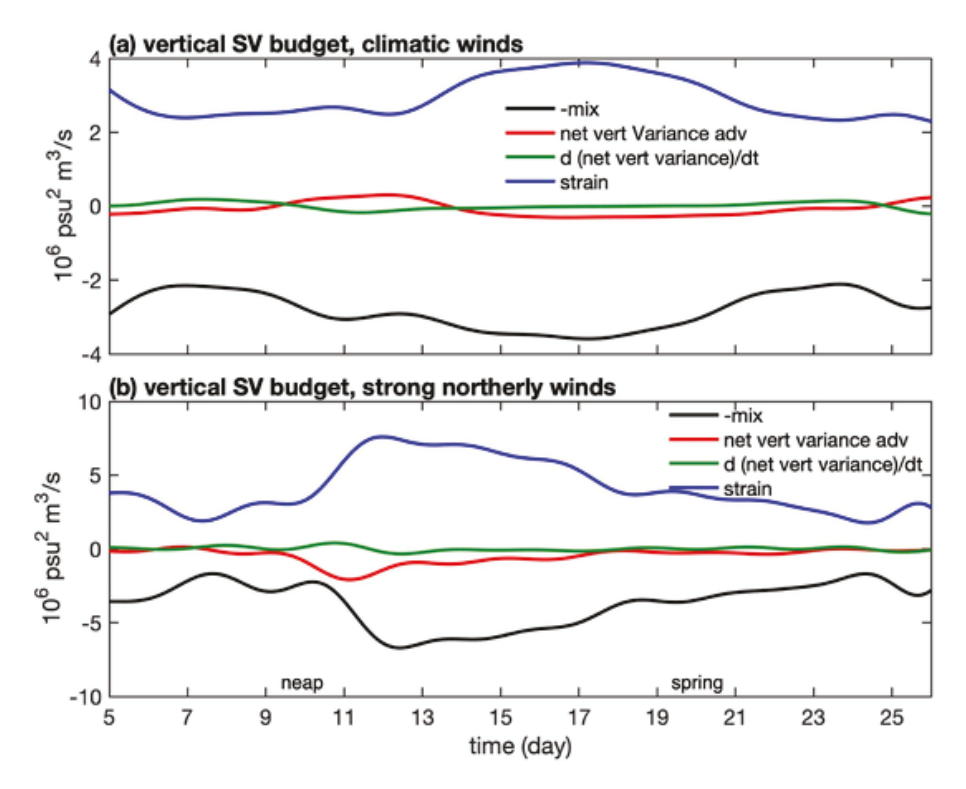


Fig. 13. Terms in the vertical SV budget (Equation (10)) in the whole estuary under climatic (a) and (b) strong northerly winds.

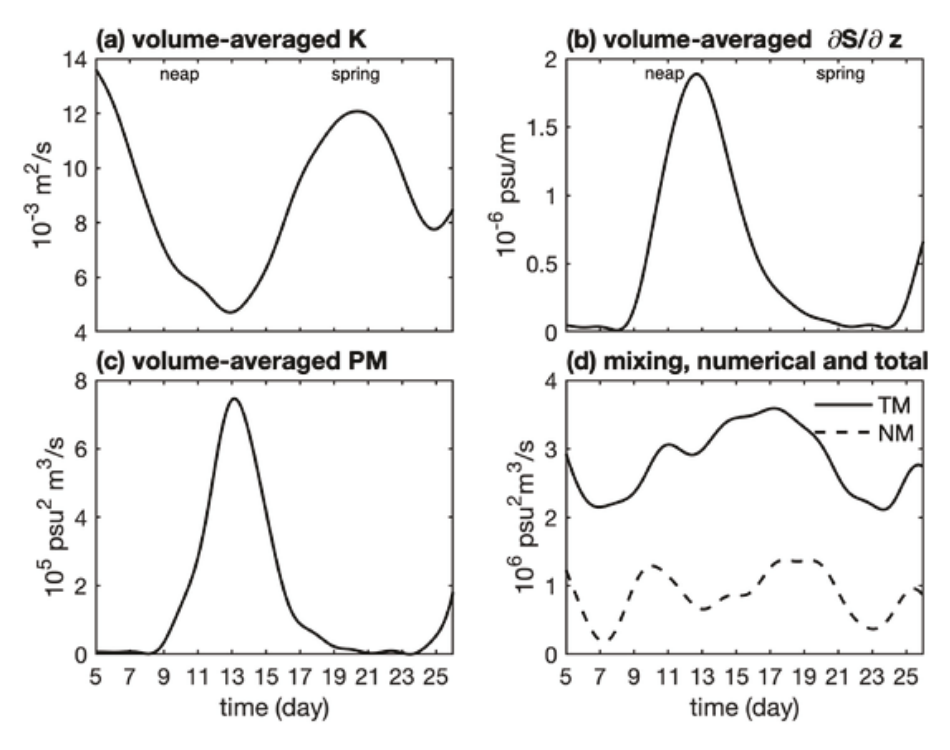


Fig. 14. Volume-averaged (a) eddy diffusivity, (b) $\partial S/\partial z$, and (c) volume-integrated physical mixing in the NC. (d) total and numerical mixing (TM, NM; solid and dashed lines). Terms in a-d are 60-h low-pass filtered from Ex1 results. Mixing terms in (d) are integrated in all channels.

However, the proportion of numerical mixing in this study is higher than that in Wang et al. (2021). The reason is that our model domain only includes the Changjiang Estuary, and the domain in Wang et al. (2021) contains the entire Bohai Sea, Yellow Sea, and East China Sea (including the Changjiang Estuary). Due to the strong river flow in the Changjiang Estuary, the volume-averaged salinity gradient is much higher than the volume-averaged salinity gradient over Bohai Sea, Yellow Sea, and East China Sea.

4.2. Future work

In this study, we use $\left(S_{v}^{\prime2}\right)_{in}$ and $\left(S_{v}^{\prime2}\right)_{out}$ to calculate the contribution of vertical SV fluxes at the boundaries. Note that the flux-weighted vertical SV considers both stratification and lateral variations across the boundaries. This will lead some errors especially when the lateral variation is comparable to the stratification. For example, during

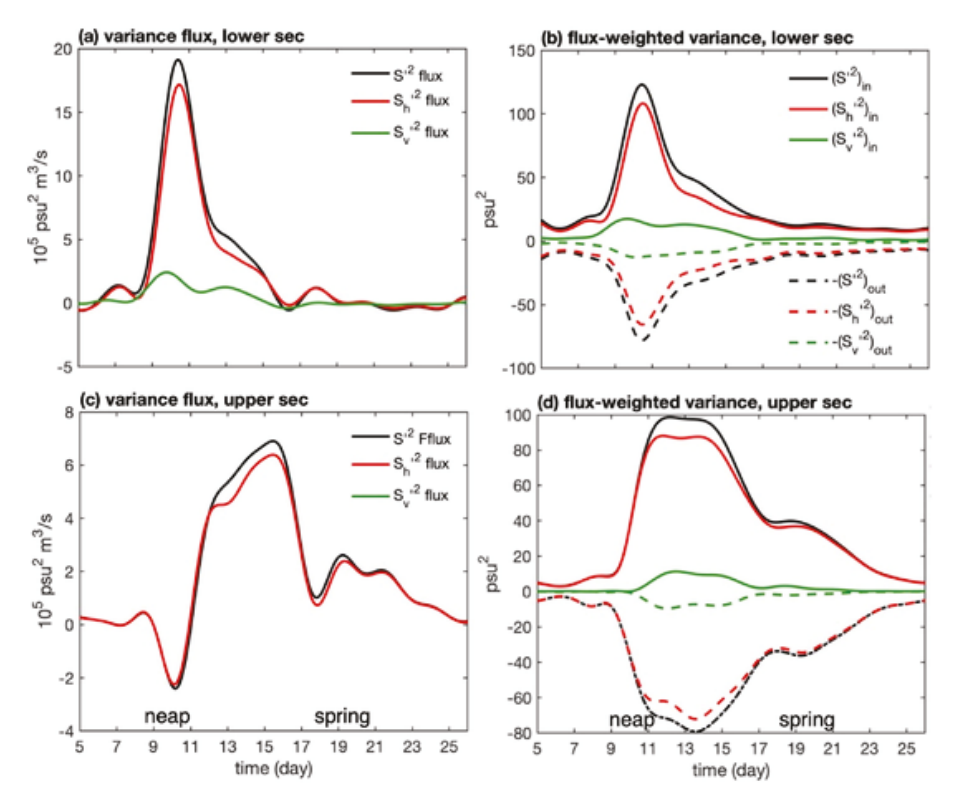


Fig. 10. As in Fig. 6, but under the strong, northerly winds of February 2014.

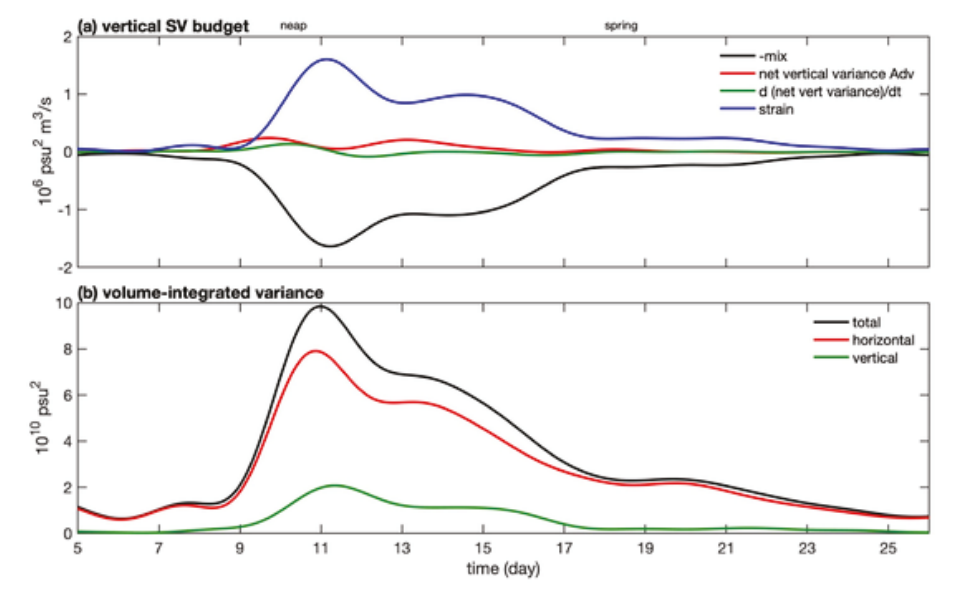


Fig. 11. (a)Terms in the vertical SV budget in the NC under strong north wind. (b) Time series of volume-integrated SV.

spring tide, the stratification is small and lateral variation will contribute most of the vertical SV flux in the NC, which will cause a bigger error. But all of the lateral, vertical and along-channel salinity gradients in the NC is very small during the spring tide, which will not change the main findings of this study. Future work could separate the lateral and vertical variation at the boundaries, and employ Eulerian coordinates rather than isohaline.

Even though we have studied the effects of strong northerly winds on SV dynamics, the effects of surface waves have not been studied and should be evaluated in the future. In addition, the effect of wind straining (Chen and Sanford, 2009; Scully et al., 2005) on the vertical SV balance has not been examined and merits further discussion.

5. Conclusions

In the previous study, the flux-weighted total SV is evaluated using the approximation $(S'^2)_{in} \approx (S_{in} - \langle \bar{S} \rangle)^2$ with the assumption of uniform inflow and outflow salinities(MacCready et al., 2018; Wang and Geyer, 2018). We now remove this assumption and make an exact rela-

tion
$$(S'^2)_{in} = (S_{in} - \langle \overline{S} \rangle)^2 + \frac{\left\langle \int_{A^+} (S - S_{in})^2 \frac{\partial Q}{\partial s} ds \right\rangle}{Q_{in}}$$
 (Equation(s 7)–(9)).

 $\frac{\left\langle \int_{A^+} (S-S_{in})^2 \frac{\partial Q}{\partial s} ds \right\rangle}{Q_{in}} \text{ is the flux-weighted vertical SV } \left(S_{v}^{\prime 2}\right)_{in} \text{in the isohaline}$

TEF framework. The benefits of change depend heavily on the salinity

gradients at the chosen boundaries. When the chosen boundaries have a stronger stratification, this improvement is worthy.

Under climatic wind in the winter, the vertical SV flux in the NC is larger than the horizontal SV flux during the early neap tide, which may be common for estuaries with landward salt fluxes dominated by estuarine circulation salt fluxes (e.g., Hudson River Estuary (Bowen and Geyer, 2003; Lerczak et al., 2006)). The horizontal SV flux dominates the SV flux at the late neap tide. Both the vertical and horizontal SV disappear during the spring tide because the salt is fully flushed back into the coastal sea. The SV flux is dominated by advection at the Lower boundary of the box, i.e., the mouth of the NC. The inward horizontal SV advection into the NC at the Upper boundary occurs later after the salt flux enters the box through the Lower boundary during neap tide. It is found that the maximum $(S_v^2)_{in}$ is 25 ps μ^2 whereas the maximum $(S_v^{\prime 2})_{out}$ is 15 ps μ^2 , which means the water with higher vertical stratification entering the box is mixed in the box and returns with lower vertical stratification to the coastal ocean. The advection (during early neap tide), straining (during late neap tide) and mixing are the dominant terms in the vertical SV balance, the rate of change in the net vertical SV is not a dominant term. The maximum mixing is 8.39×10^5 (psu² m³/s) appearing at the late neap tide when the volume-integrated vertical SV reaches the maximum and eddy diffusivity reaches the minimum.

Under the strong north wind in February 2014, saline water with a relatively weak stratification is advected into the NC. As a result, the contribution of advection of vertical SV at the Lower section decreases significantly and the advection of horizontal SV increases. The advection of horizontal SV under the strong north wind is about 2 times of that under the climatic wind. Volume-integrated mixing and SV in the NC also increase under the strong north wind. The landward transport in the NC prevents the river discharge from entering into NC. As a result, more river discharge enters into the southern channels, which increases the stratification at the mouth of South Passage and North Passage. This process induces an export of vertical SV in the South Passage and North Passage.

CRediT authorship contribution statement

Linjiang Li: Conceptualization, Methodology, Validation, Formal analysis, Writing – original draft. **Jianrong Zhu:** Software, Writing – review & editing, Supervision. **L. Fernando Pareja-Roman:** Writing – review & editing, Formal analysis.

Declaration of competing interest

The authors declare that they have no known competing financial interests or personal relationships that could have appeared to influence the work reported in this paper.

Acknowledgments

Linjiang Li was supported by the Zhuhai Basic and Applied Basic Research Foundation (ZH22017003200004PWC). Jianrong Zhu was supported by the National Natural Science Foundation of China (41676083). L. Fernando Pareja-Roman was supported by the U.S. National Science Foundation (PREEVENTS program, award 1855037). We acknowledge Robert Chant and Chuning Wang for fruitful discussions. All data sets used in this study are available at https://figshare.com/s/10c76b8c52c94b5cc06b. Anonymous reviewers helped improve the manuscript and discussion. The authors declare no competing interests.

Appendix A. Derivation of Equations (9) and (10)

Equation (9) can be proven as follows:

$$\begin{split} S_{in} &= \frac{Fs_{in}}{Q_{in}} \\ S_{in} &= \frac{\left\langle \int_{A^{+}} S^{2} \frac{\partial Q}{\partial s} ds \right\rangle}{Q_{in}} \\ \left\langle \int_{A^{+}} S^{2} \frac{\partial Q}{\partial s} ds \right\rangle - Q_{in} S_{in}^{2} = \left\langle \int_{A^{+}} S^{2} \frac{\partial Q}{\partial s} ds \right\rangle \\ &+ Q_{in} S_{in}^{2} - 2S_{in} \left\langle \int_{A^{+}} S^{2} \frac{\partial Q}{\partial s} ds \right\rangle \\ \left\langle \int_{A^{+}} S^{2} \frac{\partial Q}{\partial s} ds \right\rangle - Q_{in} S_{in}^{2} = \left\langle \int_{A^{+}} S^{2} \frac{\partial Q}{\partial s} ds \right\rangle + \\ \left\langle \int_{A^{+}} S^{2} \frac{\partial Q}{\partial s} ds \right\rangle - Q_{in} S_{in}^{2} = \left\langle \int_{A^{+}} (S - S_{in})^{2} \frac{\partial Q}{\partial s} ds \right\rangle \\ \left\langle \int_{A^{+}} S^{2} \frac{\partial Q}{\partial s} ds \right\rangle - Q_{in} S_{in}^{2} = \left\langle \int_{A^{+}} (S - S_{in})^{2} \frac{\partial Q}{\partial s} ds \right\rangle \\ \left\langle \int_{A^{+}} S^{2} \frac{\partial Q}{\partial s} ds \right\rangle + Q_{in} \left\langle \overline{S} \right\rangle^{2} - 2Q_{in} S_{in} \left\langle \overline{S} \right\rangle \\ - Q_{in} \left\langle \overline{S} \right\rangle^{2} + 2Q_{in} S_{in} \left\langle \overline{S} \right\rangle - Q_{in} S_{in}^{2} = \\ \left\langle \int_{A^{+}} (S - S_{in})^{2} \frac{\partial Q}{\partial s} ds \right\rangle \\ - Q_{in} \left(S_{in} - \left\langle \overline{S} \right\rangle \right)^{2} = \left\langle \int_{A^{+}} (S - S_{in})^{2} \frac{\partial Q}{\partial s} ds \right\rangle \\ - Q_{in} \left(S_{in} - \left\langle \overline{S} \right\rangle \right)^{2} = \left\langle \int_{A^{+}} (S - S_{in})^{2} \frac{\partial Q}{\partial s} ds \right\rangle - 2 \left\langle \overline{S} \right\rangle \\ \left\langle \int_{A^{+}} S^{2} \frac{\partial Q}{\partial s} ds \right\rangle + \left\langle \overline{S} \right\rangle^{2} \left\langle \int_{A^{+}} \frac{\partial Q}{\partial s} ds \right\rangle - 2 \left\langle \overline{S} \right\rangle \\ \left\langle \int_{A^{+}} S^{2} \frac{\partial Q}{\partial s} ds \right\rangle + \left\langle \int_{A^{+}} \left\langle \overline{S} \right\rangle^{2} \frac{\partial Q}{\partial s} ds \right\rangle - \left\langle \int_{A^{+}} 2 \left\langle \overline{S} \right\rangle S \frac{\partial Q}{\partial s} ds \right\rangle - Q_{in} \left(S_{in} - \left\langle \overline{S} \right\rangle \right)^{2} = \\ \left\langle \int_{A^{+}} (S - S_{in})^{2} \frac{\partial Q}{\partial s} ds \right\rangle - Q_{in} \left(S_{in} - \left\langle \overline{S} \right\rangle \right)^{2} \\ = \left\langle \int_{A^{+}} (S - S_{in})^{2} \frac{\partial Q}{\partial s} ds \right\rangle - Q_{in} \left(S_{in} - \left\langle \overline{S} \right\rangle \right)^{2} \\ = \left\langle \int_{A^{+}} (S - S_{in})^{2} \frac{\partial Q}{\partial s} ds \right\rangle - Q_{in} \left(S_{in} - \left\langle \overline{S} \right\rangle \right)^{2} \\ = \left\langle \int_{A^{+}} (S - S_{in})^{2} \frac{\partial Q}{\partial s} ds \right\rangle - Q_{in} \left(S_{in} - \left\langle \overline{S} \right\rangle \right)^{2} \\ = \left\langle \int_{A^{+}} (S - S_{in})^{2} \frac{\partial Q}{\partial s} ds \right\rangle - Q_{in} \left(S_{in} - \left\langle \overline{S} \right\rangle \right)^{2} \\ = \left\langle \int_{A^{+}} (S - S_{in})^{2} \frac{\partial Q}{\partial s} ds \right\rangle - Q_{in} \left(S_{in} - \left\langle \overline{S} \right\rangle \right)^{2} \\ = \left\langle \int_{A^{+}} (S - S_{in})^{2} \frac{\partial Q}{\partial s} ds \right\rangle - Q_{in} \left(S_{in} - \left\langle \overline{S} \right\rangle \right)^{2} \\ = \left\langle \int_{A^{+}} (S - S_{in})^{2} \frac{\partial Q}{\partial s} ds \right\rangle - Q_{in} \left(S_{in} - \left\langle \overline{S} \right\rangle \right)^{2} \\ = \left\langle \int_{A^{+}} (S - S_{in})^{2} \frac{\partial Q}{\partial s} ds$$

$$\left\langle \frac{\int_{A^{+}} \left(S - \left\langle \overline{S} \right\rangle \right)^{2} \frac{\partial Q}{\partial s} ds}{Q_{in}} \right\rangle - \left(S_{in} - \left\langle \overline{S} \right\rangle \right)^{2}$$

$$= \frac{\left\langle \int_{A^{+}} \left(S - S_{in} \right)^{2} \frac{\partial Q}{\partial s} ds \right\rangle}{Q_{in}}$$

$$\left(S^{\prime 2} \right)_{in} = \left(S_{h}^{\prime 2} \right)_{in} + \left(S_{v}^{\prime 2} \right)_{in}$$

References

- Aristizabal, M., Chant, R., 2013. A numerical study of salt fluxes in Delaware bay estuary. J. Phys. Oceanogr. 43, 1572–1588.
- Atlas, E.B. f. M., 1992. Ocean Atlas in Huanghai Sea and East China Sea (Hydrology). China Ocean Beijing.
- Blumberg, A., 1994. In: A Primer for Ecom-Si, vol. 66. Technical report of HvdroOual.
- Bowen, M.M., Geyer, W., 2003. Salt transport and the time-dependent salt balance of a partially stratified estuary. Journal of Geophysical Research-Oceans 108.
- Burchard, H., Rennau, H., 2008. Comparative quantification of physically and numerically induced mixing in ocean models. Ocean Model. 20, 293–311.
- Chen, S.-N., Geyer, W.R., Ralston, D.K., Lerczak, J.A., 2012. Estuarine exchange flow quantified with isohaline coordinates: contrasting long and short estuaries. J. Phys. Oceanogr. 42, 748–763.
- Chen, S.-N., Sanford, L.P., 2009. Axial wind effects on stratification and longitudinal salt transport in an idealized, partially mixed estuary. J. Phys. Oceanogr. 39, 1905–1920.
- Geyer, W.R., MacCready, P., 2014. The estuarine circulation. Annu. Rev. Fluid Mech. 46, 175–197.
- Giddings, S., MacCready, P., 2017. Reverse estuarine circulation due to local and remote wind forcing, enhanced by the presence of along-coast estuaries. J. Geophys. Res.: Oceans 122, 10184–10205.
- Gong, W., Shen, J., 2011. The response of salt intrusion to changes in river discharge and tidal mixing during the dry season in the modaomen estuary, China. Continent. Shelf Res. 31, 769–788.
- Gräwe, U., Naumann, M., Mohrholz, V., Burchard, H., 2015. Anatomizing one of the largest saltwater inflows into the baltic Sea in december 2014. J. Geophys. Res.: Oceans 120, 7676–7697.
- Hansen, D.V., Rattray, M., 1965. Gravitational circulation in straits and estuaries. J. Mar. Res. 23, 104-122.
- Lerczak, J.A., Geyer, W.R., Chant, R.J., 2006. Mechanisms driving the timedependent salt flux in a partially stratified estuary. J. Phys. Oceanogr. 36, 2296–2311.
- Li, L., Zhu, J., Chant, R.J., Wang, C., Pareja-Roman, L.F., 2020. Effect of dikes on saltwater intrusion under various wind conditions in the Changjiang estuary. Journal of Geophysical Research-Oceans 125.
- Li, L., Zhu, J., Wu, H., 2012. Impacts of wind stress on saltwater intrusion in the yangtze estuary. Sci. China Earth Sci. 55, 1178-1192.
- Li, L., Zhu, J., Wu, H., Guo, Z., 2014. Lateral saltwater intrusion in the north channel of the Changiang estuary. Estuar. Coast 37, 36-55.
- Li, L., Zhu, J., Wu, H., Wang, B., 2010. A numerical study on water diversion ratio of the Changjiang (yangtze) estuary in dry season. Chin. J. Oceanol. Limnol. 28, 700–712.
- Li, M., Zhong, L., Boicourt, W.C., Zhang, S., Zhang, D.L., 2006. Hurricane-induced storm surges, currents and destratification in a semi-enclosed bay. Geophys. Res. Lett. 33.
- Li, X., Geyer, W.R., Zhu, J., Wu, H., 2018. The transformation of salinity variance: a new approach to quantifying the influence of straining and mixing on estuarine stratification. J. Phys. Oceanogr. 48, 607–623.
- Lyu, H., Zhu, J., 2018. Impact of the bottom drag coefficient on saltwater intrusion

- in the extremely shallow estuary. J. Hydrol. 557, 838-850.
- Lyu, H., Zhu, J., 2019. Impacts of tidal flat reclamation on saltwater intrusion and freshwater resources in the Changjiang estuary. J. Coast Res. 35, 314–321.
- MacCready, P., 2011. Calculating estuarine exchange flow using isohaline coordinates. J. Phys. Oceanogr. 41, 1116–1124.
- MacCready, P., Geyer, W.R., Burchard, H., 2018. Estuarine exchange flow is related to mixing through the salinity variance budget. J. Phys. Oceanogr. 48, 1375–1384.
- Mellor, G.L., Yamada, T., 1982. Development of a turbulence closure model for geophysical fluid problems. Rev. Geophys. 20, 851–875.
- Monismith, S.G., Kimmerer, W., Burau, J.R., Stacey, M.T., 2002. Structure and flow-induced variability of the subtidal salinity field in northern san francisco bay. J. Phys. Oceanogr. 32, 3003–3019.
- Purkiani, K., Becherer, J., Klingbeil, K., Burchard, H., 2016. Wind-induced variability of estuarine circulation in a tidally energetic inlet with curvature. J. Geophys. Res.: Oceans 121, 3261–3277.
- Ralston, D.K., Geyer, W.R., 2019. Response to channel deepening of the salinity intrusion, estuarine circulation, and stratification in an urbanized estuary. J. Geophys. Res.: Oceans 124 (7), 4784–4802. https://doi.org/https://.org/10.1029/2018JC014313.
- Rayson, M.D., Gross, E.S., Hetland, R.D., Fringer, O.B., 2017. Using an isohaline flux analysis to predict the salt content in an unsteady estuary. J. Phys. Oceanogr. 47, 2811–2828.
- Rennau, H., 2011. Natural, Numerical and Structure-Induced Mixing in Dense Gravity Currents: Idealised and Realistic Model Studies.
- Scully, M.E., Friedrichs, C., Brubaker, J., 2005. Control of estuarine stratification and mixing by wind-induced straining of the estuarine density field. Estuaries 28, 321–326.
- Simpson, J.H., Brown, J., Matthews, J., Allen, G., 1990. Tidal straining, density currents, and stirring in the control of estuarine stratification. Estuaries 13, 125–132.
- Sutherland, D.A., MacCready, P., Banas, N.S., Smedstad, L.F., 2011. A model study of the salish Sea estuarine circulation. J. Phys. Oceanogr. 41, 1125–1143.
- Wang, D.-P., 1979. Wind-driven circulation in the chesapeake bay, winter, 1975. J. Phys. Oceanogr. 9, 564–572.
- Wang, T., Geyer, W.R., 2018. The balance of salinity variance in a partially stratified estuary: implications for exchange flow, mixing, and stratification. J. Phys. Oceanogr. 48, 2887–2899.
- Wang, T., Geyer, W.R., MacCready, P., 2017. Total exchange flow, entrainment, and diffusive salt flux in estuaries. J. Phys. Oceanogr. 47, 1205–1220.
- Wang, T., Wei, Z., Jiang, W., Xu, T., Chen, J.-L., Bian, C., 2021. Quantification of numerical mixing in coastal ocean models through an offline method. Ocean Engineering 222 108588.
- Wu, H., Zhu, J., 2010. Advection scheme with 3rd high-order spatial interpolation at the middle temporal level and its application to saltwater intrusion in the Changjiang estuary. Ocean Model. 33, 33–51.
- Wu, H., Zhu, J., Choi, B.H., 2010. Links between saltwater intrusion and subtidal circulation in the Changjiang estuary: a model-guided study. Continent. Shelf Res. 30, 1891–1905.
- Xue, P., Chen, C., Ding, P., Beardsley, R.C., Lin, H., Ge, J., Kong, Y., 2009.
 Saltwater intrusion into the Changjiang River: a model-guided mechanism study. J. Geophys. Res.: Oceans 114.
- Zhang, E.F., Gao, S., Savenije, H.H.G., Si, C.Y., Cao, S., 2019. Saline water intrusion in relation to strong winds during winter cold outbreaks: north Branch of the yangtze estuary. J. Hydrol. 574, 1099–1109.
- Zhu, J., Cheng, X., Li, L., Wu, H., Gu, J., Lyu, H., 2020. Dynamic mechanism of an extremely severe saltwater intrusion in the Changjiang estuary in february 2014. Hydrol. Farth Syst. Sci. 24, 5043–5056.